Journal of Magnetic Resonance **144,** 175–185 (2000)
doi:10.1006/jmre.2000.2064, available online at http://www.idealibrary.com on IDEAL®

An Iterative Fitting Procedure for the Determination of Longitudinal NMR Cross-Correlation Rates

Lincong Wang,* Alexander V. Kurochkin,* and Erik R. P. Zuiderweg*,†,‡

*Biophysics Research Division, †Department of Biological Chemistry, and ‡Department of Chemistry, University of Michigan, Ann Arbor, Michigan 48109

Received September 3, 1999; revised February 18, 2000

We present a method to measure ^{15}N–^{1}H dipolar/^{15}N CSA longitudinal cross-correlation rates in protonated proteins. The method depends on the measurement of four observables: the cumulative proton–proton cross relaxation rates, the ^{15}N R_1 relaxation rate, the multiexponential decay of $2N_ZH_Z^N$ spin-order, and multiexponential buildup of $2N_ZH_Z^N$ spin-order. The ^{15}N–^{1}H dipolar/^{15}N CSA longitudinal cross-correlation rate is extracted from these measurements by an iterative fitting procedure to the solution of differential equations describing the coupled relaxation dynamics of the *z*-magnetization of the ^{15}N nucleus, the two-spin-order $2N_ZH_Z^N$, and a two-spin-order term $2N_ZH_Z^Q$ describing the interaction with remote protons. The method is applied to the microbial ribonuclease binase. The method can also extract longitudinal cross-correlation rates for those amide protons that are involved in rapid solvent exchange. The experiment that serves for extracting proton–proton cross-relaxation rates is a modification of 3D ^{15}N-resolved NOESY-HSQC. The experiment restores the solvent magnetization to its equilibrium state during data detection for all phase cycling steps and all values of NOE mixing times and is recommended for use in standard applications as well. © 2000 Academic Press

Key Words: **relaxation interference; chemical shift anisotropy; NOESY; proteins; dynamics.**

The importance of internal motions for the biochemical functions of proteins has been well documented. Modern NMR techniques, capable of measuring the relaxation rates of various spin coherences for many sites in a protein under physiological conditions, have provided much of the available information about such motions (for a review, see Ref. (*1*)). Most NMR studies have focused on individual spins such as the backbone amide nitrogen (^{15}N) and on the dipolar (DD) interaction with its attached proton. Recently, many studies have appeared that measure different cross-correlated relaxation rates. Cross correlations measure the interference of two relaxation mechanisms and give insight into the existence of correlated motions of vectors, into local structure, and into the properties of CSA tensors. Cross correlations also provide powerful tools for measuring dynamical properties, because the theoretical relationship between the cross-correlation rates and the spectral density functions is simple. This is especially the case when interference is measured for transverse relaxation pathways (R_2). Even for the complex spin relaxation networks occurring in proteins, cross-correlation experiments can be designed so that the relaxation can be described with a high degree of accuracy as a two-spin system. In fact, such R_2 cross correlations "isolate" a restricted set of relaxation mechanisms out of a complex relaxation matrix. These properties thus allow detailed insight into the structure and dynamics of labeled proteins, and recent years have seen a flurry of such measurements, many of which measure R_2 interference effects of CSA and dipolar interactions (*2–9*).

Recently interest has arisen to also measure R_1 interference effects of CSA and dipolar relaxation, mostly to obtain R_2/R_1 ratios for the ^{15}N–^{1}H CSA-DD cross correlations in proteins. Such ratios should allow a valuable estimate of the spectral density functions independent of ^{15}N CSA tensor values and conformational dynamics (R_{ex}) relaxation. As described early by Torchia and co-workers (*10*), R_1 interference effects are much more difficult to measure than R_2 interference rates. For instance, the ^{15}N–^{1}H dipolar/^{15}N CSA longitudinal cross *correlation* as measured from the time-dependence of $2N_ZH_Z^N$ order is strongly affected by cross *relaxation* of the ^{1}H spin with other ^{1}H spins, which is for proteins a dominant effect. (Why this does not influence R_2 cross correlations as measured from the time-dependence of $2N^+H_Z$ coherence is recalled in detail in Refs. (*3*) and (*9*)). In other words, R_1 cross correlations do not fully isolate a restricted set of relaxation mechanisms and cannot be measured in straightforward manner in spin-dense systems such as proteins. Moreover, NH moieties for which the amide protons are in relatively rapid exchange (1-s time scale) with the solvent can also not be described by a simple two-spin system.

Here we present a theoretical description of the relaxation behavior of a three-spin system which serves as a model for the ^{15}N–^{1}H system in contact with another ^{1}H relaxation and mass exchange bath. On the basis of the theoretical investigation, we suggest that with the measurement of four observables (the individual proton–proton cross-relaxation and exchange rates, the ^{15}N R_1 relaxation rate, the multiexponential $2N_ZH_Z^N$ decay, and multiexponential $2N_ZH_Z^N$ buildup), it is possible to obtain the longitudinal ^{15}N–^{1}H CSA-DD cross-correlation rates by iterative fitting of the latter data according to coupled differential equations. Our analysis indicates that reliable R_1 cross-

1090-7807/00 $35.00

correlation rates can be measured with this approach for fully protonated proteins while mass exchange mechanisms such as amide proton exchange with the solvent are taken into account as well. We have applied our procedure with experimental data for the microbial ribonuclease binase (12.3 kDa).

Our method, in which the ^1H–^1H cross relaxation is *measured*, complements recent work by Palmer and co-workers (*11*), who propose to *attenuate* the ^1H–^1H cross relaxation in longitudinal ^{15}N–^1H CSA-DD cross correlation by deuteration of all nonamide protons, and by Bodenhausen and co-workers (*12*) who propose to *attenuate* the ^1H–^1H cross relaxation by off-resonance spin-locking.

THEORY

Following Goldman (*13*) we use the master Eq. [1] for relaxation in the interaction representation as derived by Abragam (*14*) to calculate the relaxation behavior of different spin orders in a three-spin system,

$$\frac{d}{dt}\langle A\rangle = -\frac{1}{2}\sum_i \int_{-\infty}^{+\infty} \mathrm{Tr}\{\overline{[[A,\, H_i(0)],\, H_i(\tau)](\sigma - \sigma_L)}\}d\tau, \quad [1]$$

where A, σ, σ_L, and H_i are, respectively, the spin operator whose evolution is to be evaluated, the reduced density operator for the spin system, its value at equilibrium state, and the interaction Hamiltonian between the spin system and the bath responsible for the relaxation of the spin system. Here, Tr indicates taking the trace over the spin system. The bar in [1] represents ensemble average.

We evaluate the dynamics of the spin system consisting of an amide proton, H^N, amide nitrogen, N, and a third proton, H^Q, that may represent all other protons, including solvent. The interaction Hamiltonian H_i for this system,

$$H_i = H^N_{CSA} + H^{H^N}_{CSA} + H^{H^Q}_{CSA} + H^{NH^N}_{DD} + H^{NH^Q}_{DD} + H^{H^NH^Q}_{DD}, \quad [2]$$

includes CSA interactions for all spins (H^N_{CSA}, $H^{H^Q}_{CSA}$, and $H^{H^N}_{CSA}$) and the DD interactions between any two of the three spins ($H^{NH^N}_{DD}$, $H^{NH^Q}_{DD}$, and $H^{H^NH^Q}_{DD}$), where

$$H^X_{CSA} = \frac{1}{3}\gamma_X(\sigma^X_\parallel - \sigma^X_\perp)\xi \sum_{q=-2}^{+2} Y^0_2(\Omega')Y^{-q}_2(\Omega(t))T^q_2(\mathbf{B}_0, X) \quad [3a]$$

and

$$H^{XY}_{DD} = -\gamma_X\gamma_Y\hbar r^{-3}_{XY}\xi \sum_{q=-2}^{+2} Y^0_2(\Omega')Y^{-q}_2(\Omega_{NH^N}(t))T^q_2(X, Y), \quad [3b]$$

where the normalization constant $\xi = (24\pi/5)^{1/2}$; γ's are the gyromagnetic ratios; r's the averaged internuclear distances; Y^{-q}_2 and T^{-q}_2 second-rank spherical harmonics tensors; N, H^N, and H^Q single spin operators; Ω's the Euler angles, and $\mathbf{B}_0$ the external static field. The $Y^0_2(\Omega')$ in Eq. [3] is the only remaining component of Wigner's rotation matrix describing the corresponding directions of the CSA or DD interactions in a molecular-fixed frame. The other components are disregarded as usual according to group-theoretical arguments. For the sake of simplicity we have assumed that all the three CSAs are axially symmetric.

The longitudinal relaxation behavior of N, H^N, and H^Q is completely described in a space spanned by the basis set {N_z, H^N_Z, H^Q_Z, $2N_zH^N_Z$, $2N_zH^Q_Z$, $2H^N_ZH^Q_Z$, $4N_zH^N_ZH^Q_Z$} of longitudinal one-, two-, and three-spin orders. The dynamics of individual spin orders is dominated by dipolar and CSA autorelaxation processes (ρ_X). Transfer of population between spin orders of the same rank is governed by dipolar cross-relaxation and chemical exchange processes (σ_{XY}). Transfer of population between spin orders of different ranks is caused by dipolar/CSA ($\eta^{DD-CSA}_{N-NH^N}$), which we want to obtain, and dipolar/dipolar cross-correlation processes. The differential equations governing all of these processes are represented by the complete cross-relaxation/cross-correlation matrix in Table 1, obtained by straightforward but tedious algebra. We have neglected all the zero-quantum terms such as $N_+H^N_-$, $N_-H^N_+$, and $H^Q_-H^N_+$ because no spin-locking field was applied during the relaxation delay. The derived formulas relating the various autorelaxation, cross-relaxation, and cross-correlation rates to the spectral density functions are given in the Appendix; the longitudinal cross-correlation rate of interest is given by

$$\eta^{DD-CSA}_{N-NH^N} = \frac{\mu_0\hbar B_0\gamma_H\gamma^2_N}{4\pi r^3_{NH}}(\sigma^N_\parallel - \sigma^N_\perp)P_2(\cos\theta)J(\omega_N), \quad [4]$$

where the symbols have their usual meanings. The theoretical values of all elements of the above matrix were computed for a three-spin geometry corresponding to an α-helical conformation in deuterated proteins (see Fig. 1), using a correlation time of 6.0 ns, which corresponds to that of binase. The values of $Y^0_2(\Omega')$ in Eq. [3] were assumed to be 1 in the calculation. The spectral density function $J(\omega)$ was assumed to be $2\tau_c/(5(1 + \omega^2\tau^2_c))$. The results of this calculation are shown in Table 2. It is clear that the complete relaxation matrix for the longitudinal spin orders can for this system be approximated, to very good extent, in a block-diagonal form on the subspaces {H^N_Z, H^Q_Z}, {$2H^N_ZH^Q_Z$}, and {N_z, $2N_zH^N_Z$, $2N_zH^Q_Z$, $4N_zH^N_ZH^Q_Z$}. As we currently are interested in dipole/CSA cross correlations, only the last subspace is relevant and the matrix describing its complete dynamics can be reduced to a 4×4 size. As described below, we center our experiments around measuring the creation and relaxation of $2N_zH^N_Z$ two-spin order. In such experiments, $4N_zH^N_ZH^Q_Z$ spin order is created as a second-order process only

TABLE 1

The Complete Longitudinal Relaxation Matrix for a Three-Spin System N, H^N, and H^Q, Accounting for Autorelaxation Rates, Cross-Relaxation Rates, and Cross-Correlation Rates Based on Dipolar/Dipolar and Dipolar/CSA Interference Effects

	Nz	H_Z^N	H_Z^Q	$2NzH_Z^N$	$2NzH_Z^Q$	$2H_Z^NH_Z^Q$	$4NzH_Z^NH_Z^Q$
Nz	ρ_N	σ_{N-H^N}	σ_{N-H^Q}	$\eta_{N-NH^N}^{DD-CSA}$	$\eta_{N-NH^Q}^{DD-CSA}$	0	$\delta_{N-NH^NH^Q}^{DD-DD}$
H_Z^N		ρ_{H^N}	$\sigma_{H^N-H^Q}$	$\eta_{H^N-NH^N}^{DD-CSA}$	0	$\eta_{H^N-H^NH^Q}^{DD-CSA}$	$\delta_{H^N-NH^NH^Q}^{DD-DD}$
H_Z^Q			ρ_{H^Q}	0	$\eta_{H^Q-NH^Q}^{DD-CSA}$	$\eta_{H^Q-H^NH^Q}^{DD-CSA}$	$\delta_{H^Q-NH^NH^Q}^{DD-DD}$
$2NzH_Z^N$				ρ_{2NH^N}	$\delta_{N-NH^NH^Q}^{DD-DD} + \sigma_{H^N-H^Q}$	$\delta_{H^N-NH^NH^Q}^{DD-DD} + \sigma_{N-H^Q}$	$\eta_{N-NH^Q}^{DD-CSA} + \eta_{H^N-H^NH^Q}^{DD-CSA}$
$2NzH_Z^Q$					ρ_{2NH^Q}	$\delta_{H^Q-NH^NH^Q}^{DD-DD} + \sigma_{N-H^Q}$	$\eta_{N-2NH^N}^{DD-CSA} + \eta_{H^Q-H^NH^Q}^{DD-CSA}$
$2H_Z^NH_Z^Q$						$\rho_{2H^NH^Q}$	$\eta_{H^Q-NH^Q}^{DD-CSA} + \eta_{H^N-NH^N}^{DD-CSA}$
$4NzH_Z^NH_Z^Q$							$\rho_{4NH^NH^Q}$

Note. The expressions for these rates are given in the Appendix.

through ^1H–^1H cross relaxation $2N_zH_Z^N \rightarrow 2N_zH_Z^Q$, followed by (mostly) ^1H–^1H dipolar cross correlation $2N_zH_Z^Q \rightarrow 4N_zH_Z^NH_Z^Q$. Consequently, when short relaxation times are used in both the experiment monitoring the decay of $2N_zH_Z^N$ (100 ms) and the experiment monitoring the magnetization transfer from N_Z to $2N_zH_Z^N$ (400 ms), the amount of $4N_zH_Z^NH_Z^Q$ spin order created can be neglected and does not contribute to the dynamics of the system. Accordingly, the cross-relaxation/cross-correlation dynamics of the subspace $\{N_z, 2N_zH_Z^N, 2N_zH_Z^Q\}$ can be described by a 3×3 matrix or the following closed set of three equations:

$$\begin{aligned}
\frac{d}{dt}\langle N_z(t)\rangle &= -\rho_N\langle N_z(t) - N_Z(\mathrm{eq})\rangle \\
&\quad + \eta_{N-NH^N}^{DD-CSA}\langle 2H_Z^N N_z(t)\rangle \\
\frac{d}{dt}\langle 2H_Z^N N_z(t)\rangle &= -(\rho_N + \sigma_{H^N-H^Q})\langle 2H_Z^N N_z(t)\rangle \\
&\quad + \eta_{N-NH^N}^{DD-CSA}\langle N_z(t) - N_Z(\mathrm{eq})\rangle \\
&\quad + \sigma_{H^N-H^Q}\langle 2H_Z^Q N_z(t)\rangle \\
\frac{d}{dt}\langle 2H_Z^Q N_z(t)\rangle &= -(\rho_N + \rho_{H^Q})\langle 2H_Z^Q N_z(t)\rangle \\
&\quad + \sigma_{H^N-H^Q}\langle 2H_Z^N N_z(t)\rangle, \qquad [5]
\end{aligned}$$

where ρ_N is the longitudinal relaxation rate of amide nitrogen (N_Z), $\eta_{N-NH^N}^{DD-CSA}$ the longitudinal cross-correlation rates measuring the interference between the DD interaction of amide nitrogen with its attached proton and the CSA of amide nitrogen with the external field that we wish to obtain, ρ_{H^Q} the longitudinal relaxation rate of the second proton (H^Q), and $\sigma_{H^N-H^Q}$ the longitudinal cross-relaxation or exchange rate of two protons. The autorelaxation rate of the two-spin-order $2N_zH_Z^N$ should be $\rho_N + \rho_{H^N}$. However, we have replaced it with $\rho_N + \sigma_{H^N-H^Q}$ because for large biomolecules the theoretical value of ρ_{H^N} is very close to the $\sigma_{H^N-H^Q}$ value. We have adopted the set of Eqs. [5] also as the basis for the extraction of the longitudinal cross-correlation rate $\eta_{N-NH^N}^{DD-CSA}$ in fully protonated proteins. In such systems every backbone amide proton interacts with many other protons including solvent. The resulting complete cross-relaxation/cross-correlation matrix becomes obviously intractable with thousands of terms even for small proteins. We have therefore assumed that the effect of all other protons was additive. As a result we replace the proton H^Q in Eqs. [5] with one pseudo-proton to mimic the effects of all the others, and the ρ_Q approximates its effective longitudinal relaxation rate.

On the basis of the above theoretical considerations, we design the following protocol to obtain the desired longitudinal cross-correlation rates $\eta_{N-NH^N}^{DD-CSA}$. The autorelaxation rate ρ_N is measured using a standard ^{15}N relaxation experiment. The cumulative cross-relaxation rate $\sigma_{H^N-H^Q}$ can be obtained from the initial decay rates of the diagonals in a 3D ^{15}N-resolved NOESY-HSQC experiment, as described below. The dynamics of $2NzH^Nz$ decay and $2NzH^Nz$ buildup is measured with two experiments. Their multiexponential time profiles are fitted according to Eqs. [5] using the appropriate initial conditions. The fitting procedure yields the value for $\eta_{N-NH^N}^{DD-CSA}$ and also the cumulative longitudinal relaxation rate ρ_{H^Q}.

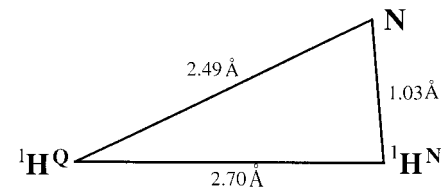

FIG. 1. A three-spin system consisting of an amide nitrogen (^{15}N), its valence-bonded amide proton ($^1H^N$), and another proton ($^1H^Q$) in α-helical conformation. The distances shown here between the ^{15}N and $^1H^Q$ and between $^1H^N$ and $^1H^Q$ were the averages of 10 such distances in 0.8-Å resolution X-ray structure of Crambian (PDB code cbn), respectively. The $^1H^Q$ was the proton closest to both the amide ^{15}N and $^1H^N$ in the helical regions of deuterated proteins.

TABLE 2
The Auto Longitudinal Relaxation Rates of One-Spin, Two-Spin-Order, and Three-Spin-Order and the Cross-Relaxation and the Cross-Correlation Rates of a Three-Spin System as Shown in Fig. 1

	Nz	H_Z^N	H_Z^Q	$2NzH_Z^N$	$2NzH_Z^Q$	$2H_Z^NH_Z^Q$	$4NzH_Z^NH_Z^Q$
Nz	**2.60**	0.06	<0.001	***−2.01***	0.07	0	−0.14
H_Z^N		**0.99**	*−0.88*	0.01	0	−0.008	0.008
H_Z^Q			**0.90**	0	0.001	−0.007	−0.002
$2NzH_Z^N$				**3.45**	*−1.02*	0.008	0.06
$2NzH_Z^Q$					**3.50**	0.06	***−2.02***
$2H_Z^NH_Z^Q$						0.12	0.02
$4NzH_Z^NH_Z^Q$							**2.57**

Note. The calculations were based on the following values: B_0 = 500 MHz (11.74 T), τ_C = 6.0 ns, $\Delta\sigma_N$ = 170 ppm (CSA of amide nitrogen ^{15}N, assumed to be axially symmetric). $\Delta\sigma_H$ = 10 ppm (CSA of amide proton ^{1}H, assumed to be axially symmetric). The relative large values are shown in bold for longitudinal, italic for cross relaxation between protons, and bold italic for cross correlation between DD and CSA of amide nitrogen and proton. The units are s^{-1}.

APPLICATION

NMR Experiments

All spectra were acquired on a Bruker AMX500 NMR spectrometer using 0.9 mM ^{15}N-labeled binase in 20 mM sodium acetate with 90% H_2O and 10% D_2O, pH 5.2. The resonance assignments were extended from the literature (*15*).

The longitudinal autorelaxation rate ρ_N of amide nitrogen (^{15}N) was measured with a standard 2D heteronuclear NMR experiment using inversion recovery (*10*). A train of 180° pulses (5-ms delay between two consecutive ones) was applied during the relaxation delay to eliminate the magnetization transfer from Nz to $2N_ZH_Z^N$ with rate $\eta_{N-NH^N}^{DD-CSA}$, comparable to ρ_N (Table 2). Consequently, the decay curves for different residues can be fitted to single exponentials, the results serving as a fixed parameter for Eqs. [5].

The decay of longitudinal two-spin-order $2N_ZH_Z^N$ for the individual residues of binase was monitored by the pulse sequence shown in Fig. 2A. No additional pulses were applied during the relaxation delay. The longest relaxation delay was set to 100 ms. These decays cannot be fitted to single exponentials and are fitted according to Eqs. [5].

The magnetization transfer from Nz to $2N_ZH_Z^N$ by $\eta_{N-NH^N}^{DD-CSA}$ for the individual residues of binase was monitored by the pulse sequence shown in Fig. 2B. No RF pulses were applied during the relaxation delay. The longest relaxation delay was set to 400 ms. These buildup curves cannot be represented by single exponentials and are fitted according to Eqs. [5].

The longitudinal cross relaxation $\sigma_{H^N-H^Q}$ of one amide proton with all of its neighbors, including amide proton exchange, can be measured from the initial decay of the diagonal peaks in a carefully arranged 3D ^{15}N-resolved NOESY-HSQC experiment (Fig. 2C) as a function of the NOE mixing time, τ_m, as follows. Generalizing the Solomon equation for the amide proton H^N that cross relaxes with many protons H^i and exchanges with the solvent H^{H_2O}, one has, neglecting proton–proton cross-correlation effects (*16*),

$$\frac{dH_z^N(\tau_m)}{d\tau_m} = -[K_{H^N,H_2O}^{ex} + \sum_i \rho_{H^N,H^i}]\{H_z^N(\tau_m) - H_z^N(eq)\} + \sum_i \sigma_{H^N,H^i}\{H_z^i(\tau_m) - H_z^i(eq)\} + K_{H^N,H_2O}^{ex}\{H_z^{H_2O}(\tau_m) - H_z^{H_2O}(eq)\}, \quad [6]$$

where the rates ρ_{H^N,H^i} and σ_{H^N,H^i} are the autorelaxation and cross-relaxation rates due to dipolar interactions between spins

FIG. 2. (A) Pulse sequence for monitoring the decay of two-spin-order $2NzH^Nz$. Narrow and wide bars denote 90° and 180° hard pulses, respectively. Open bars indicate solvent-selective pulses. Lower bars represent spin-locking pulses of 1.0 ms. All pulses were applied with phase *x* unless specified otherwise. A composite 180° pulse (90°*y*–180°*x*–90°*y*) was applied during the ^{15}N evolution. The delays were tuned for the relaxation properties of binase as follows: τ_1 = 2.55 ms and T_n = 2.67 ms. The phase cycling was: $\phi_1 = y, y, -y, -y$; $\phi_2 = x, x, x, x, -x, -x, -x, -x$; $\phi_3 = x, y, -x, -y$; receiver = $x, -x, -x, x, -x, x, x, -x$. States–TPPI was applied to ϕ_2 to achieve quadrature detection in the indirect dimension. The spectral widths were 8333 Hz for protons and 1900 Hz for ^{15}N, respectively. Heteronuclear decoupling during data acquisition was achieved with a Waltz-16 composite pulse scheme. The WATERGATE scheme was used to suppress the solvent resonance (*25*). The ^{15}N evolution could also have been measured as shown in (B). The time points for the relaxation delays were 10, 15, 20, 30, 50, 75, and 100 ms. The number of scans was 32 per FID. (B) Pulse sequence for monitoring the magnetization transfer from Nz to $2NzH^Nz$. The symbols have the same meaning as in (A) except for the following. The phase cycling was: $\phi_1 = x, -x$; $\phi_2 = x, x, x, x, x, x, x, x, -x, -x, -x, -x, -x, -x, -x, -x$; $\phi_3 = x, x, y, y, -x, -x, -y, -y$; $\phi_4 = y$; receiver = $x, -x, -x, x$. States–TPPI was applied to ϕ_4 to achieve quadrature detection in the indirect dimension. The time points for the relaxation delays were 50, 75, 100, 150, 200, 300, and 400 ms. The number of scans was 128 per FID. (C) Pulse sequences for the determination of the ρ_{H^N} values, which correspond to the cumulative amide proton cross-relaxation rates $\sigma_{H^N-H^Q}$. The symbols have the same meaning as in (A) except for the following. Prior to the gradient G3, four solvent-selective square 45° pulses of approximately 500 μs each

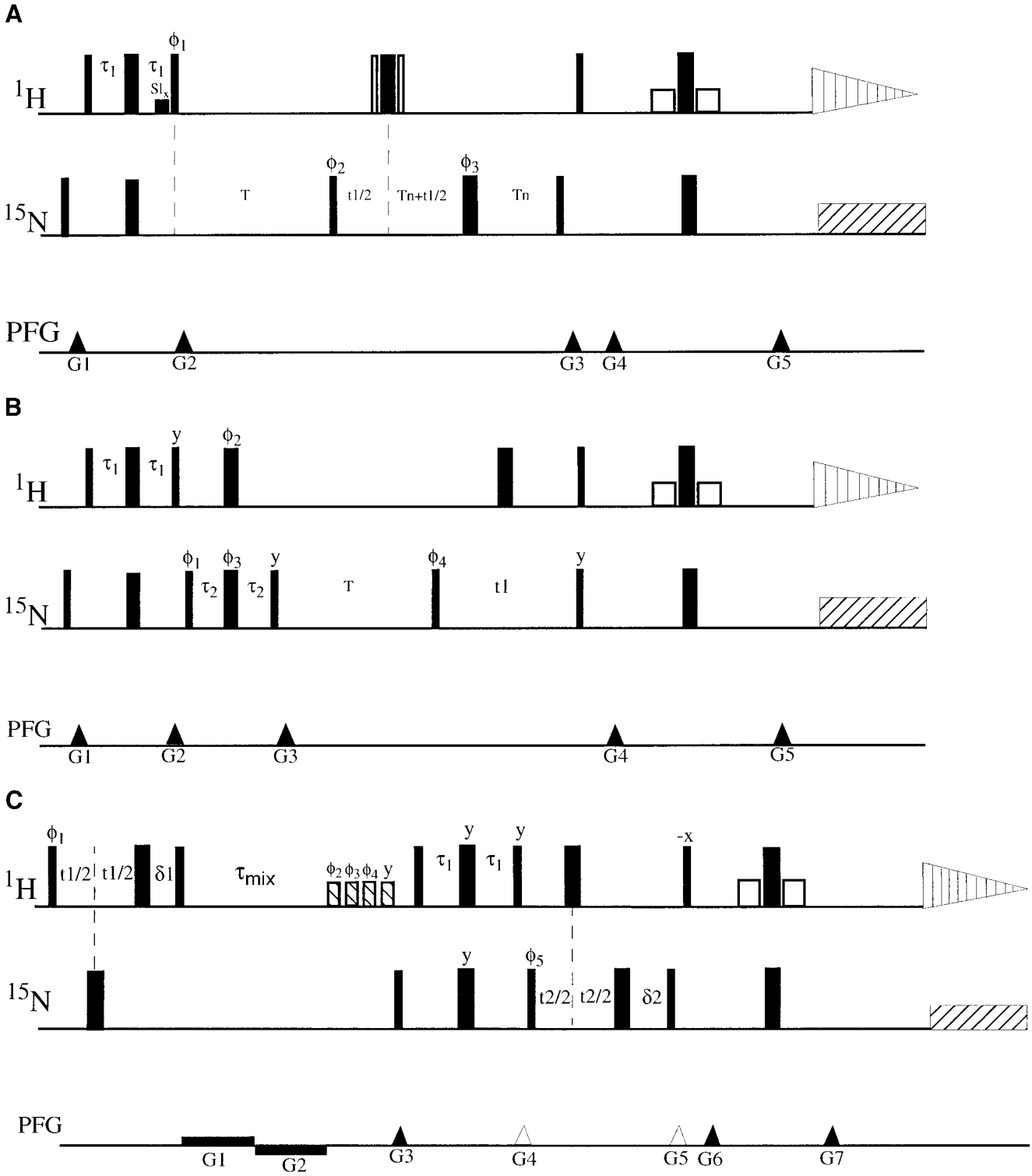

(indicated by hatched boxes) were applied to restore the "water-up" condition. τ_1 = 2.75 ms. $\phi_1 = x, x, -x, -x$; $\phi_2 = y$, $\phi_3 = \phi_4 = -y, -y, y, y$; $\phi_5 = x, -x$; receiver = $x, -x, -x, x$. States–TPPI was applied to ϕ_1 and ϕ_5 to achieve quadrature detection in the indirect dimensions. The phase program ϕ_2 was incremented by 180° for each 90° ϕ_1 States–TPPI incrementation, and programs ϕ_3 and ϕ_4 were incremented by 180° for every two 90° States–TPPI incrementations of ϕ_1 to restore water-up conditions. The gradients G1, G2, G3, G6, and G7 were 1, −1, 12, 40, and 40 G/cm, respectively. The gradients G4 and G5 are optional and serve to suppress radiation damping for long ^{15}N evolution times, but were not used in this study. The delays δ_1 and δ_2, together with the π pulses in the indirection evolution times, serve to suppress first-order phase shifts and were set to the initial delay t_1 + ^{15}N π-pulse width and initial delay t_2 + ^{1}H π-pulse length, respectively. The time points for the relaxation delays were 10, 15, 20, 30, 50, 75, and 100 ms. The number of scans was 16 per FID.

H^N and H^i, respectively, and $K^{ex}_{H^N,H_2O}$ the amide-proton–solvent exchange rate.

The initial dynamics of diagonal peaks $\{H^N\}$ in NOESY spectra corresponds to that of selectively inverted resonances $\{H^N\}$, with all other magnetizations $\{H^i\}$ at their equilibrium values (*17*). Accordingly, for small values of the NOE mixing time, we have $H^i_z(\tau_m \approx 0) - H^i_z(\text{eq}) \cong 0$, and consequently, no contribution of the second term of Eq. [6]. If the NOE experiment is arranged such that the water signal behaves like any other proton, i.e., that it is not saturated and not affected by radiation damping, it can also be considered at its equilibrium value, $H^{H_2O}_z(\tau_m \approx 0) - H^{H_2O}_z(\text{eq}) \cong 0$, and consequently the third term of Eq. [6] can also be neglected. Thus one has that the initial decay of any diagonal peak is described by a single exponential with the rate constant $K^{ex}_{H^N,H_2O} + \sum_i \rho_{H^N,H^i}$. In the large molecule limit, the autorelaxation rates ρ_{H^N,H^i} and cross-relaxation rates σ_{H^N,H^i} are equal and opposite. Accordingly the cross-relaxation rate $\sigma_{H^N-H^Q}$ in Eq. [5] is equal to $-R_D$, the initial decay rate of the diagonal of the NOESY experiment:

$$R_D = -\sigma_{H^N-H^Q} = K^{ex}_{H^N,H_2O} - \sum_i \sigma_{H^N,H^i}. \qquad [7]$$

To obtain these conditions, a NOESY experiment was designed such that no presaturation was used and such that the solvent signal behaves as any other proton signal (see Fig. 2C). The latter is achieved by applying two weak gradients with opposite signs during the NOE mixing time, preventing radiation damping, but maintaining coherence. It was assured that water is in $+z$ during detection irrespective of the phasecycling by always restoring the solvent magnetization to $+z$ prior to the fast-HSQC sequence (*18*), using a sequence of four water-selective $\pi/4$ pulses that are phase cycled to cumulatively generate 0, $\pi/2(y)$, $\pi(y)$, and $3\pi/4(y)$ pulses as needed to follow the phase and quadrature cycling of the first proton pulse of the sequence. This single experiment yields excellent water suppression, with "water-up" for all practical NOE mixing times in the range of 10–200 ms, and is also recommended for use in standard applications. Proton zero-quantum coherences of the type $(2I_xS_y - 2I_yS_x)$ will be present after the short NOE mixing time, and cannot, as is well known, be phase cycled out or purged by the gradient after the selective pulses. The NOESY-FHSQC sequence converts these coherences into *ZZ*-orders at acquisition time that do not contribute to the diagonal signal as can be verified by standard product operator algebra. Accordingly, no disturbance of the single-exponential decay behavior of the diagonals occurs.

As our current interest is to only monitor the initial decay rate of the large diagonal resonances, 3D datasets of excellent sensitivity and resolution could be acquired in as little as 10 h each, using an older 500-MHz system. As such, the acquisition of a 3D σ relaxation series with NOE mixing times of 10, 15, 20, 30, 50, 75, and 100 ms took as long as any standard 2D relaxation experiment. After 3D processing, the initial diagonal peak decay profiles were fitted with a single exponential function, yielding the desired sum of cross-relaxation and exchange rates, the results serving as a fixed parameter in Eqs. [5].

Details describing further experimental conditions and data acquisition parameters for all experiments are given in the figure legends. All data were processed and analyzed with the program NMRPipe (*19*).

The Iterative Fitting Procedure

The iterative fitting procedures were developed to extract the unknown longitudinal relaxation rate ρ_Q of the pseudo-proton H^Q and the longitudinal cross-correlation rate $\eta^{DD-CSA}_{N-NH^N}$. First, ρ_Q was estimated from the best fit of the solution of Eq. [5] to the data of the experiment monitoring the decay of the two-spin-order $2N_ZH^N_Z$ using the initial conditions $\{Nz(0) = 0; 2N_ZH^N_Z(0) = \text{the measured initial value}; 2N_ZH^Q_Z(0) = 0\}$. The three equations in (*5*) were solved numerically with the Program Mathematica 3.0 (Wolfram Research). The fit was performed by exhaustively varying ρ_Q and $\eta^{DD-CSA}_{N-NH^N}$, first within a large range and then gradually narrowing the range down step by step until the precision was equal to or better than the experimental uncertainties of the original experimental data. We found that the fit was very sensitive to the values of the cumulative autorelaxation rates ρ_Q (see Results and Discussion). However, this fit was not very sensitive to the values of the cross-correlation rate $\eta^{DD-CSA}_{N-NH^N}$.

In contrast, we found that the fitting to the experiment monitoring the magnetization transfer from Nz to $2N_ZH^N_Z$ was very sensitive to the value of the cross-correlation rate $\eta^{DD-CSA}_{N-NH^N}$, as expected, but much less so to the value of the autorelaxation rate ρ_Q. Thus, with ρ_Q values as known parameters obtained from the first fit, the cross correlation rates $\eta^{DD-CSA}_{N-NH^N}$ could be obtained to high precision by best fit of Eq. [5] to the $Nz \rightarrow 2N_ZH^N_Z$ experiment with the initial conditions $\{2N_ZH^N_Z(0) = 0; 2N_ZH^Q_Z(0) = 0\}$. Here, the initial value for Nz(0) was exhaustively varied together with $\eta^{DD-CSA}_{N-NH^N}$.

This two-step fitting procedure was tested with data simulated numerically according to Eqs. [5] with known parameters and was found to give very accurate results. In fact, it was much more robust than a simulated annealing program that was also written by us to accomplish the same fitting procedure in a more automatic fashion.

RESULTS AND DISCUSSION

We have applied the iterative fitting procedure detailed above to binase, a microbial ribonuclease, M_r 12.3 kDa. Nineteen well-resolved peaks were picked for testing the protocol. The resulting cross-correlation rates are shown in Fig. 3C. The average cross-correlation rate at 11.7 T is 2.3 s^{-1}, which compares favorably with the computed rate of 2.0 s^{-1} (Table 2) using standard parameters and a value of 6.0 ns for the rotational correlation time obtained from routine ^{15}N relaxation

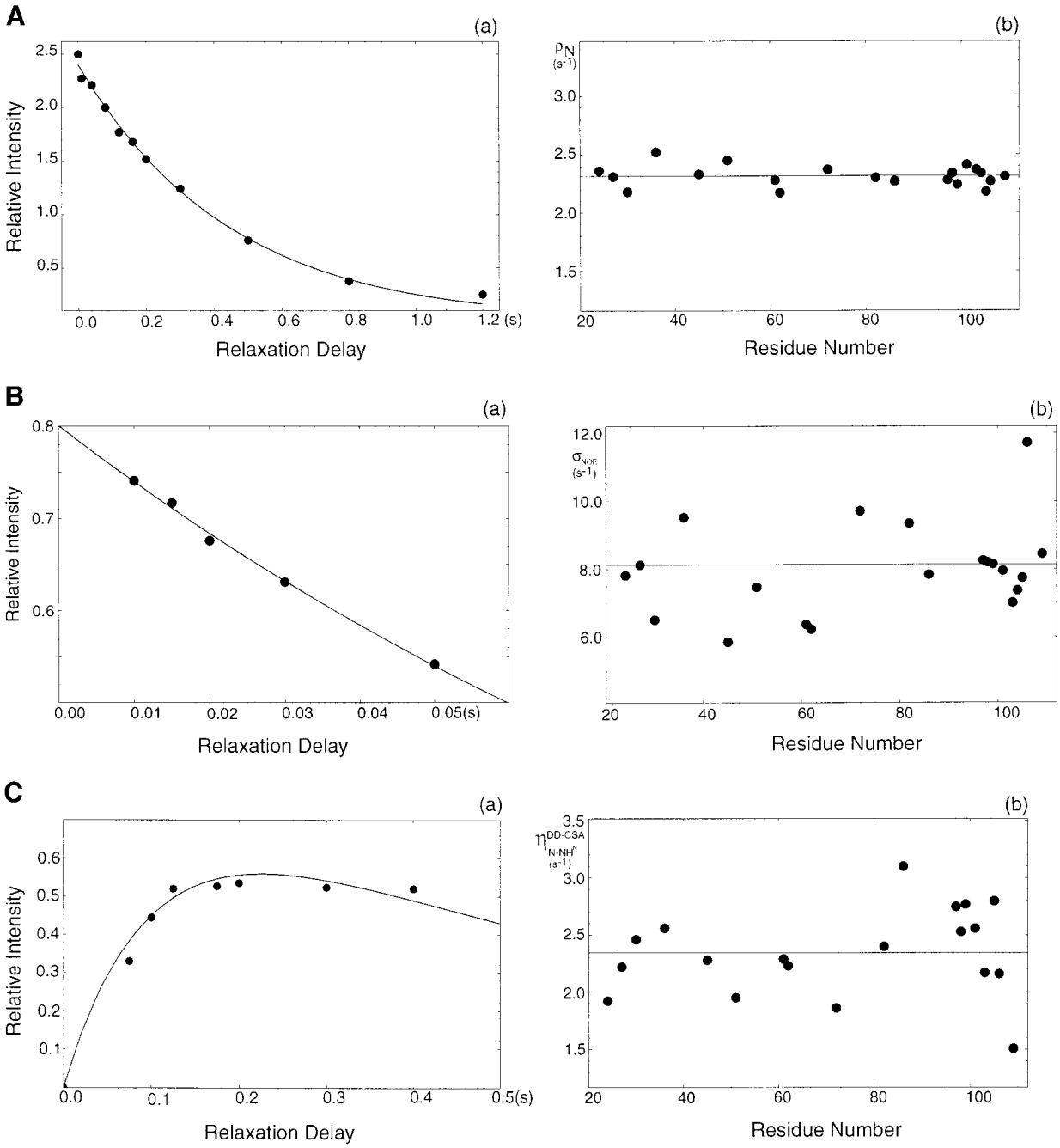

FIG. 3. A. (a) Representative experimental data of the ^{15}N T_1 experiment, using cross-correlation suppression (*26*), for residue R86 of binase and the fit to a single exponential decay curve. The *x*-axis is the relaxation time in seconds; the *y*-axis is the relative peak intensity. (b) The fitted ρ_N (R_1) values of the amide nitrogen ^{15}N for 19 residues of binase. B. (a) Representative experimental data of the relaxation in the 3D ^{15}N-resolved NOESY experiment (Fig. 2C) for residue R86 of binase and the fit to a single exponential decay curve. The *x*-axis is the mixing time in seconds; the *y*-axis is the relative peak intensity. (b) The fitted ρ_{H^N} values of the amide protons for 19 residues of binase. C. (a) Representative experimental data of the experiment (Fig. 2B) residue R86 of binase, which monitors the magnetization transfer from Nz to $2H^NzNz$ and the fitting to the solution of the Eq. [5] by the iterative procedure. (b) The fitted cross-correlation rates $\eta_{N-NH^N}^{DD-CSA}$ for 19 residues of binase.

experiments. The measured cross correlation rates vary largely in the range of 1.6–2.8 s^{-1} and do not correspond to patterns in either hydrogen bonding or secondary structure. As is detailed directly below, the large range of values observed cannot be attributed to statistical errors in the experimental observables or errors in the fitting procedure. Our results are complementary to those of many other studies by several groups reporting determinations of different cross-correlation rates. For many

such experiments, larger variations than expected are observed as well. The explanations for this phenomenon vary from ascribing a large range to the parameters of the static CSA tensors (*6*), variations in geometry (*20*), anisotropic local motions (*21*), and, most recently, dynamic variations in the CSA tensors and distances upon anisotropic local motion (*22*). Analysis of the current data in structural and dynamical terms will thus have to await further developments of these theories. The purpose of the present paper is only to provide a robust protocol to measure the longitudinal cross-correlation rates. In the following we address the error propagation in the procedure. Subsequently we compare our method with that recently published by Kroenke *et al.* (*11*).

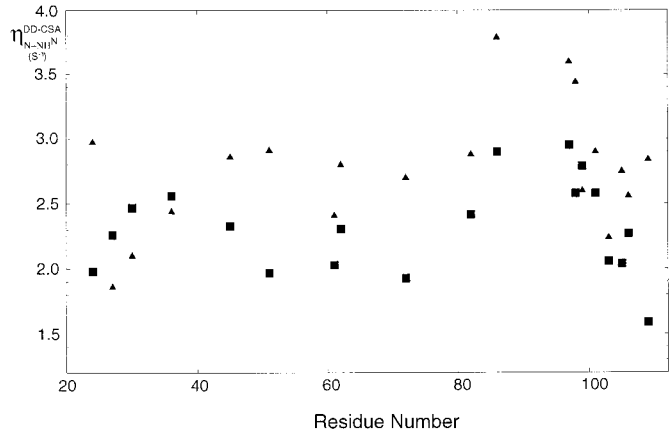

FIG. 4. The fitted cross-correlation rates $\eta_{N-NH^N}^{DD-CSA}$ of 19 residues of binase as obtained by our iterative protocol (filled squares) compared with those as determined with the protocol described by Kroenke *et al.* (*11*) (filled triangles).

Errors Analysis

Errors in ρ_N. The pulse train is the standard ^{15}N ρ measurement does not eliminate the magnetization transfer from Nz to $4N_ZH_Z^NH_Z^Q$ by dipole/dipole cross correlation. However, the rate of such transfer $\delta_{N-NH^NH^Q}^{DD-DD}$ can be calculated to be relatively small, about 5% of ρ_N with the presence of one other proton (see Table 2), and should not affect the early parts of the relaxation curve. Fitting such a curve to a single exponential would yield an error in ρ_N of at most 2.5%.

The uncertainty in ρ_N due to the noise in the original experimental data is small. The average signal-to-noise ratio was about 100/2. Since the autorelaxation rates ρ_N were extracted by best fitting of 12 data points to single exponential decaying curves, the uncertainty in ρ_N is estimated to be less than 0.8%. Combined with the error in neglecting the $\delta_{N-NH^NH^Q}^{DD-DD}$ terms, we estimate that the error in ρ_N is 3%.

Errors in $\sigma_{H^N-H^Q}$. The NOESY diagonal peaks were also obtained with an average sensitivity of 100/2. With a fit to five data points the experimental uncertainty in $\sigma_{H^N-H^Q}$ is less than 1.0%. Potential sources of systematic errors in obtaining the cross-relaxation rates are discussed in the theoretical section of this paper. We note that the decay curves cannot be distinguished from single exponentials even when extended to 100-ms mixing times; nevertheless we have only fitted up to 50 ms, to maintain the initial rate approximation. We estimate that the sum of experimental and systematic error in the derived values for $\sigma_{H^N-H^Q}$ is well below 10%.

Errors in the fitted parameters ρ_Q and $\eta_{N-NH^N}^{DD-CSA}$. The experimental uncertainties in the experiment monitoring the decay of $2NzH^Nz$ was about 100/1 for the initial time point and 100/2 for the last of seven time points. The signal to noise ratio in the transfer experiment Nz to $2NzH^Nz$ was on average 100/5 for seven time points. The experimental uncertainties of parameters fitted to these data should thus be reduced by $\sqrt{7}$ compared to the raw individual data points. The computational uncertainties in ρ_N, ρ_Q, and $\eta_{N-NH^N}^{DD-CSA}$ were estimated by sample fitting procedures in which the other parameters and observables were varied over their known uncertainty ranges. We found that a 3% error in ρ_N contributes less than a 2% error in the final computed $\eta_{N-NH^N}^{DD-CSA}$ value. It was observed that the error in ρ_Q is dominated by potential variations in the initial value of the $2NzH^Nz$ magnetization. We estimate on this basis an error in ρ_Q as large as 25% from the first step of the fitting procedure. However, a 25% error in ρ_Q introduces only a 2% error in the desired cross-correlation rate $\eta_{N-NH^N}^{DD-CSA}$ in the second fitting procedure. To explain this more intuitively, we note that ρ_Q affects the time dependence of $2NzH^Nz$ only indirectly through the decay of the $2NzH^Qz$ term (see Eqs. [5]). In particular, for the $2NzH^Nz$ decay experiment, the $2NzH^Qz$ term has to be created first from $2NzH^Nz$ before it can contribute "back" to $2NzH^Nz$, a process that is unimportant if the relaxation time is only 100 ms as used. The influence of the H^Q relaxation is even more remote on the transfer experiment from Nz to $2NzH^Nz$ (400 ms); it can be classified as a secondary to secondary effect: first, $2NzH^Nz$ is created from Nz, then $2NzH^Qz$ is created from $2NzH^Nz$. Only $2NzH^Qz$ is directly affected by ρ_Q. The largest computational error in the cross-correlation rate $\eta_{N-NH^N}^{DD-CSA}$ was caused by the uncertainties in the initial values of Nz used as the input parameter in the second fitting procedure. A reasonable estimate of 5% error in the initial value of Nz would introduce 5% error in $\eta_{N-NH^N}^{DD-CSA}$. In total, we thus estimate that the uncertainties in $\eta_{N-NH^N}^{DD-CSA}$ amount to 15% on average. These cumulative experimental and computational uncertainties can thus not account for the large spread of cross correlation rates obtained ($\pm$50%).

Comparison with Other Work

As detailed above in the theoretical background, the relaxation behavior of any spin residing in the complicated network of spins, especially in a protonated protein sample, may not be approximated by a two-by-two matrix without introducing substantial errors. For example, by fitting the experimental data of residue R86 of binase to a two-by-two matrix, we obtain $\eta_{N-NH^N}^{DD-CSA}$ of 3.32 s^{-1}. By contrast, it was found to be 3.10 s^{-1} by

TABLE 3

The Difference in Longitudinal Cross-Correlation Rates $\eta_{N-NH^N}^{DD-CSA}$ as Determined with the Iterative Fitting Procedure Proposed Here and with the Method Proposed by Kroenke *et al.* (*11*)

Residue	$\Delta\eta_{N-NH^N}^{DD-CSA}$ (s^{-1})	Structure	Exchange
I24	1.1	Loop	Yes
S27	−0.4	Loop/helix	No
S30	−0.4	Loop/helix	Yes
A36	−0.1	Loop	No
A45	0.6	Helix/turn	No
G51	1.0	Beta	Yes
R61	0.1	Loop	No
L62	0.5	Loop	No
E72	0.9	Beta	Yes
R82	0.5	Loop	No
R86	0.8	Beta	No
K97	0.9	Beta	No
T98	0.9	Beta	No
T99	−0.2	Loop	[a]
H101	0.3	Loop	No
A103	0.1	Loop	No
F105	−0.6	Loop	[b]
T106	0.4	Beta	No
R109	1.3	Beta	[c]

Note. The column "Structure" characterizes the local structure in the protein binase (G. Dodson, personal communication); the column "Exchange" indicates whether amide proton exchange on the 100-ms timescale was observed for this moiety.

[a] Not Determined; X-ray structure shows H-bonding.

[b] Not determined; X-ray structure shows solvent exposure.

[c] Not determined; C-terminal residue.

our iterative fitting procedure. To further explore this experimentally, we have measured and computed the longitudinal cross-correlation rates $\eta_{N-NH^N}^{DD-CSA}$ for protonated binase according to the protocol described by Kroenke *et al.* (*11*). The results are included in Fig. 4. As is expected for this protonated protein, these rates do differ substantially from the results obtained with our method. While we have not been able to find any correlation between the *values* of the cross-correlation rates and the structure of binase (see above), we do find a substantial correlation between the *differences* in the rates obtained according to our methods and those as determined by the methods of Kroenke *et al.* (*11*). As seen in Table 3, the largest differences occur for residues located in β-sheet and those involved in rapid amide proton exchange. This can be rationalized by the fact that in β-sheet, amide protons are very close to the α-protons of the preceding residues (2.2 Å); as such the relaxation dynamics of the amide proton is dominated by dipolar interaction with this single proton. The relaxation behavior is thus expected to deviate strongly from the isolated spin approximation. Large differences are also expected for amide protons in rapid exchange with the solvent, where a two-spin description cannot be a good approximation. The differences appear less strong for residues in α-helices and loops; this can be rationalized by the fact that the relaxation is not dominated by a single spin but by several other amide protons and many side-chain protons. In that case, magnetization transferred from amide proton to such protons rapidly diffuses in the matrix and the process contributes predominantly to the autorelaxation terms.

Perdeuteration of the amino acid side chains can of course alleviate some of the multiple spin effects. This method was proposed by Kroenke *et al.* (*11*). However, cross relaxation between amide protons, dominant in α-helical segments, and exchange with solvent cannot be accounted for with such an approach. Alternatives to deuteration exist, as cross relaxation between amide and aliphatic protons can be quenched by block or selective decoupling of the aliphatic protons (*23, 24*). But, as above, it is not possible to quench the amide–amide proton cross relaxation with this method. In principle, amide–amide proton cross relaxation can be attenuated strongly in the elegant approach described by Bodenhausen and co-workers (*12*). There, ^{1}H–^{1}H cross relaxation is canceled by off-resonance ^{1}H spin-locking at an average angle of 35.3°. In the large-molecule motional limit complete suppression should occur at precisely this angle (NOESY-ROESY cancellation). However, amide proton exchange effects cannot be canceled by the spin-locking schema, while RF offsets make it difficult to meet the ideal locking angle for all resonances simultaneously.

Our method to obtain the longitudinal cross-correlation rates $\eta_{N-NH^N}^{DD-CSA}$, albeit also an approximation, can be used on fully protonated proteins. A drawback is that the data must be fitted carefully to a set of coupled differential equations. This may be a small price to pay in order to also obtain information on residues involved in relatively fast amide proton exchange. Many times such residues are located in loop regions which are often the most interesting from a dynamical as well as functional perspective.

APPENDIX

The various relaxation rate constants in Table 1 were derived from Eqs. [1]–[3] and are

$$\begin{aligned}\rho_N = {} & d_{NH}^2(6J(\omega_N) + 2J(\omega_H - \omega_N) + 12J(\omega_H + \omega_N)) \\ & + d_{NQ}^2(6J(\omega_N) + 2J(\omega_Q - \omega_N) \\ & + 12J(\omega_Q + \omega_N)) + C_N^2 6J(\omega_N)\end{aligned}$$

$$\begin{aligned}\rho_{H^N} = {} & d_{NH}^2(6J(\omega_H) + 2J(\omega_H - \omega_N) + 12J(\omega_H + \omega_N)) \\ & + d_{HQ}^2(6J(\omega_H) + 2J(\omega_H - \omega_Q) \\ & + 12J(\omega_H + \omega_Q)) + C_H^2 6J(\omega_H)\end{aligned}$$

$$\begin{aligned}\rho_{H^Q} = {} & d_{NQ}^2(6J(\omega_Q) + 2J(\omega_Q - \omega_N) + 12J(\omega_Q + \omega_N)) \\ & + d_{HQ}^2(6J(\omega_H) + 2J(\omega_H - \omega_Q) \\ & + 12J(\omega_H + \omega_Q)) + C_Q^2 6J(\omega_Q)\end{aligned}$$

$$\rho_{2NH^N} = d_{NH}^2(6J(\omega_N) + 6J(\omega_H)) + d_{HQ}^2(6J(\omega_H) + 2J(\omega_H - \omega_Q) + 12J(\omega_H + \omega_Q)) + d_{NQ}^2(6J(\omega_N) + 2J(\omega_Q - \omega_N) + 12J(\omega_Q + \omega_N)) + C_N^2 6J(\omega_N) + C_H^2 6J(\omega_Q)$$

$$\rho_{2NH^Q} = d_{NQ}^2(6J(\omega_N) + 6J(\omega_Q)) + d_{HQ}^2(6J(\omega_H) + 2J(\omega_H - \omega_Q) + 12J(\omega_H + \omega_Q)) + d_{NH}^2(6J(\omega_N) + 2J(\omega_H - \omega_N) + 12J(\omega_H + \omega_N)) + C_N^2 6J(\omega_N) + C_Q^2 6J(\omega_Q)$$

$$\rho_{2H^NH^Q} = d_{HQ}^2(6J(\omega_H) + 6J(\omega_Q)) + d_{NQ}^2(6J(\omega_Q) + 2J(\omega_N - \omega_Q) + 12J(\omega_N + \omega_Q)) + d_{NH}^2(6J(\omega_H) + 2J(\omega_H - \omega_N) + 12J(\omega_H - \omega_N)) + C_H^2 6J(\omega_H) + C_Q^2 6J(\omega_Q)$$

$$\rho_{4NH^NH^Q} = d_{HN}^2(6J(\omega_N) + 6J(\omega_H)) + d_{HQ}^2(6J(\omega_H) + 6J(\omega_Q)) + d_{NQ}^2(6J(\omega_N) + 6J(\omega_Q)) + C_H^2 6J(\omega_H) + C_Q^2 6J(\omega_Q) + C_N^2 6J(\omega_N)$$

$$\sigma_{N-H^N} = d_{NH}^2(12J(\omega_H + \omega_N) - 2J(\omega_H - \omega_N))$$

$$\sigma_{N-H^Q} = d_{NQ}^2(12J(\omega_Q + \omega_N) - 2J(\omega_Q - \omega_N))$$

$$\sigma_{H^N-H^Q} = d_{HQ}^2(12J(\omega_H + \omega_Q) - 2J(\omega_H - \omega_Q))$$

$$\eta_{N-NH^N}^{DD-CSA} = 2C_N d_{NH} P_2(\cos\theta_{N-NH}) 6J(\omega_N)$$

$$\eta_{N-NH^Q}^{DD-CSA} = 2C_N d_{NQ} P_2(\cos\theta_{N-NQ}) 6J(\omega_N)$$

$$\eta_{H^N-NH^N}^{DD-CSA} = 2C_H d_{NH} P_2(\cos\theta_{H^N-NH}) 6J(\omega_H)$$

$$\eta_{H^N-H^NH^Q}^{DD-CSA} = 2C_H d_{HQ} P_2(\cos\theta_{H^N-HQ}) 6J(\omega_H)$$

$$\eta_{H^Q-NH^Q}^{DD-CSA} = 2C_Q d_{NQ} P_2(\cos\theta_{H^Q-NQ}) 6J(\omega_Q)$$

$$\eta_{H^Q-H^NH^Q}^{DD-CSA} = 2C_Q d_{HQ} P_2(\cos\theta_{H^Q-HQ}) 6J(\omega_Q)$$

$$\delta_{N-NH^NH^Q}^{DD-DD} = 2d_{NH} d_{NQ} P_2(\cos\theta_{NQ-NH}) 6J(\omega_N)$$

$$\delta_{H^N-NH^NH^Q}^{DD-DD} = 2d_{NH} d_{HQ} P_2(\cos\theta_{HQ-NH}) 6J(\omega_H)$$

$$\delta_{H^Q-NH^NH^Q}^{DD-DD} = 2d_{NQ} d_{HQ} P_2(\cos\theta_{NQ-HQ}) 6J(\omega_Q)$$

in which

$$d_{NH} = -\sqrt{\frac{1}{8}}\frac{\mu_0}{4\pi}\gamma_H\gamma_N\hbar r_{NH}^{-3},$$

$$d_{NQ} = -\sqrt{\frac{1}{8}}\frac{\mu_0}{4\pi}\gamma_Q\gamma_N\hbar r_{NQ}^{-3},$$

$$d_{HQ} = -\sqrt{\frac{1}{8}}\frac{\mu_0}{4\pi}\gamma_H\gamma_Q\hbar r_{HQ}^{-3},$$

$$C_N = \sqrt{\frac{1}{18}}\gamma_N B_0 \Delta_N,$$

$$C_H = \sqrt{\frac{1}{18}}\gamma_H B_0 \Delta_H,$$

$$C_Q = \sqrt{\frac{1}{18}}\gamma_Q B_0 \Delta_Q,$$

$$J(\omega_i) = \frac{2}{5}\frac{\tau_c}{1 + (\omega_i\tau_c)^2},$$

$$\omega_N = \gamma_N B_0, \quad \omega_H = \gamma_H B_0 \quad \text{and} \quad \omega_Q = \gamma_Q B_0.$$

The various parameters have their usual meanings, that is, μ_0 is the permeability of free space, $\hbar$ is Planck's constant divided by two times π, γ_i is the gyromagnetic ratio for nucleus i, r_{ij} is the distance between nuclei i and j, B_0 is the static magnetic field, Δ_i is the (axial) chemical shift anisotropy of nucleus i, $P_2(x) = (3x^2 - 1)/2$, θ_{i-ij} is the angle between the principal axis of the CSA tensor of nucleus i and the vector between nuclei i and j, θ_{ij-kl} is the angle between the two internuclear vectors ij and kl.

ACKNOWLEDGMENTS

This work was supported by The National Science Foundation, Grant MCB9814431. We thank Prof. Dr. Anil Kumar for stimulating discussions and Dr. Maurizio Pellecchia and Mr. Yuxi Pang for assistance with some of the NMR experiments. We thank Dr. Guy Dodson for high-resolution X-ray crystal structure coordinates of binase.

REFERENCES

1. M. W. F. Fischer, A. Majumdar, and E. R. P. Zuiderweg, Protein NMR relaxation: Theory, applications and outlook. *Prog. NMR Spectrosc.* **33,** 207–272 (1998).
2. N. Tjandra, A. Szabo, and A. Bax, Protein backbone dynamics and ^{15}N chemical shift anisotroy from quantitative measurement of relaxation interference effects. *J. Am. Chem. Soc.* **118,** 6986–6991 (1996).
3. M. W. F. Fischer, L. Zeng, Y. Pang, W. Hu, A. Majumdar, and E. R. P. Zuiderweg, Experimental characterization of models for backbone pico-second dynamics in proteins. Quantification of NMR auto- and cross correlation relaxation mechanisms involving different nuclei of the peptide plane. *J. Am. Chem. Soc.* **119,** 12629–12642 (1997).
4. B. Reif, M. Henning, and C. Griesinger, Direct measurement of angles between bond vectors in high-resolution NMR. *Science* **276,** 1230–1233 (1997).
5. D. Yang, R. Konrat, and L. E. Kay, A multidimensional NMR experiment for the measurement of the protein dihedral angle phi based on cross-correlation relaxation between Ha–Ca dipolar and C′ CSA mechanisms. *J. Am. Chem. Soc.* **119,** 11938–11940 (1998).
6. D. Fushman, N. Tjandra, and D. Cowburn, Direct measurement of ^{15}N chemical shift anisotropy in solution. *J. Am. Chem. Soc.* **120,** 10947–10952 (1998).
7. M. Tessari, F. A. A. Mulder, R. Boelens, and G. W. Vuister, Determination of amide proton CSA in ^{15}N-labeled proteins using ^{1}H

CSA/^{15}N–^{1}H dipolar and ^{15}N CSA/^{15}N–^{1}H dipolar cross-correlation rates. *J. Magn. Reson.* **127,** 128–133 (1997).

8. R. Ghose, K. Huang, and J. H. Prestegard, Measurement of cross-correlation between dipolar coupling and chemical shift anisotropy in the spin relaxation of ^{13}C, ^{15}N-labeled proteins. *J. Magn. Reson.* **135,** 487–499 (1998).
9. Y. Pang, L. Wang, M. Pellecchia, A. V. Kurochkin, and E. R. P. Zuiderweg, Evidence for extensive anisotropic local motions in a small enzyme using a new method to determine NMR cross-correlated relaxation rates in the absence of resolved scalar coupling. *J. Biomol. NMR* **14,** 297–306 (1999).
10. L. E. Kay, L. K. Nicholson, F. Delaglio, A. Bax, and D. A. Torchia, Pulse sequences for removal of the effects of cross correlation between dipolar and chemical shift anisotropy relaxation mechanisms on the measurement of heteronuclear T1 and T2 values in proteins. *J. Magn. Reson.* **97,** 359–375 (1992).
11. C. D. Kroenke, J. P. Loria, L. K. Lee, M. Rance, and A. G. Palmer III, Longitudinal and transverse ^{1}H–^{15}N dipolar/^{15}N chemical shift relaxation interference: Unambiguous determination of rotational diffusion tensors and chemical exchange effects in biological macromolecules. *J. Am. Chem. Soc.* **120,** 7905–7915 (1998).
12. I. C. Felli, H. Desvaux, and G. Bodenhausen, Local mobility of ^{15}N labeled biomolecules characterized through cross-correlation rates: Applications to paramagnetic proteins. *J. Biomol. NMR* **12,** 509–521 (1998).
13. M. Goldman, Interference effects in the relaxation of a pair of unlike spin $\frac{1}{2}$ nuclei. *J. Magn. Reson.* **60,** 437–452 (1984).
14. A. Abragam, "The Principles of Nuclear Magnetism," Clarendon Press, Oxford (1961).
15. A. V. Kurochkin, M. P. Kirpichinov, and H. Rüterjans, Studies of the spatial structure of binase in solution. Sequential resonance assignments in the 2D ^{1}H NMR spectrum. *Doklady Biochem.* **321,** 282–286 (1991).
16. I. Solomon, Relaxation processes in a system of two spins. *Phys. Rev.* **99,** 559–565 (1955).
17. R. R. Ernst, G. Bodenhausen, and A. Wokaun, "Principles of Nuclear Magnetic Resonance in One and Two Dimensions," Clarendon Press, Oxford (1987).
18. S. Mori, C. Abeygunawardana, M. O. Johnson, and P. C. M. van Zijl, Improved sensitivity of HSQC spectra of exchanging protons at short interscan delays using a new fast HSQC(FHSQC) detection scheme that avoids water saturation. *J. Magn. Reson. B* **108,** 94–98 (1995).
19. F. Delaglio, S. Grzesiek, G. W. Vuister, G. Zhu, J. Pfeifer, and A. Bax, NMRPipe: A multidimensional spectral processing system based on UNIX pipes. *J. Biomol. NMR* **6,** 277–293 (1995).
20. J. Boyd and C. Redfield, Defining the orientation of the ^{15}N shielding tensor using ^{15}N NMR relaxation data for a protein in solution. *J. Am. Chem. Soc.* **120,** 9692–9693 (1998).
21. M. W. F. Fischer, L. Zeng, A. Majumdar, and E. R. P. Zuiderweg, Characterizing semi-local motions in proteins by NMR relaxation studies. *Proc. Natl. Acad. Sci. USA* **95,** 8016–8019 (1998).
22. C. Scheurer, N. R. Skrynnikov, S. F. Lienin, R. Brüschweiler, and R. R. Ernst, Effects of dynamics and environment on ^{15}N chemical shielding anisotropy in proteins. A combination of density functional theory, molecular dynamics simulation, and NMR relaxation. *J. Am. Chem. Soc.* **121,** 4242–4251 (1999).
23. J. Fejzo, W. M. Westler, S. Macura, and J. L. Markley, Elimination of chemical-exchange-mediated spin diffusion from exchange spectra of macromolecules. Exchange-decoupled NOESY (XD-NOESY). *J. Magn. Reson.* **92,** 195–202 (1991).
24. I. Burghardt, R. Konrat, and G. Bodenhausen, Measurement of cross-correlation of fluctuations of dipolar coupling and anisotropic chemical shifts by selective spin locking. *Mol. Phys.* **75,** 467–480 (1992).
25. M. Piotto, V. Saudek, and V. Sklenar, Gradient-tailored excitation for single-quantum NMR spectroscopy of aqueous solution. *J. Biomol. NMR* **2,** 661–665 (1992).
26. J. Boyd, U. Hommel, and I. D. Campbell, Influence of cross-correlation between dipolar and anisotropic chemical shift relaxation mechanisms upon longitudinal relaxation rates of ^{15}N in macromolecules. *Chem. Phys. Lett.* **175,** 477–481 (1990).